

FEMTOSECOND TIME-RESOLVED PHOTOELECTRON SPECTROSCOPY OF POLYATOMIC MOLECULES

Albert Stolow

Steele Institute for Molecular Sciences, National Research Council of Canada, Ottawa, Ontario, Canada K1A 0R6; email: albert.stolow@nrc.ca

Key Words wavepacket, dynamics, nonadiabatic, photoionization, proton transfer

■ **Abstract** Femtosecond time-resolved photoelectron spectroscopy is emerging as a useful technique for investigating excited state dynamics in isolated polyatomic molecules. The sensitivity of photoelectron spectroscopy to both electronic configurations and vibrational dynamics makes it well suited to the study of ultrafast nonadiabatic processes. We review the conceptual interpretation of wavepacket dynamics experiments, emphasizing the role of the final state. We discuss the advantages of the molecular ionization continuum as the final state in polyatomic wavepacket experiments and show how the electronic structure of the continuum can be used to disentangle electronic from vibrational dynamics. We illustrate these methods with examples from diatomic wavepacket dynamics, internal conversion in polyenes and polyaromatic hydrocarbons, excited state intramolecular proton transfer, and azobenzene photoisomerization dynamics.

INTRODUCTION

Photoexcited polyatomic molecules often exhibit quite complex dynamics involving the redistribution of both charge and energy within the system. This coupling of charge with energy flow is understood in terms of interactions between electronic and vibrational degrees of freedom. Our notions of electronic and vibrational states originate from the Born-Oppenheimer approximation (BOA), an adiabatic separation of electronic from nuclear motions. The BOA plays the pivotal role in defining the potential energy surface that allows us to represent nuclear trajectories and thus permits a mechanistic picture of molecular dynamics. It is exact, provided that the nuclear kinetic energy is negligible. The breakdown of the BOA is uniquely caused by nuclear dynamics and occurs at the intersections or near intersections of potential energy surfaces belonging to different electronic states. The excited state dynamics of polyatomic molecules is dominated by the nonadiabatic coupling of vibrational and electronic degrees of freedom. These nonadiabatic processes are variously called radiationless transitions, electronic relaxation or

internal conversion. Such dynamics are the primary step in the photochemistry of many polyatomic molecules (1), photobiological processes such as vision and photosynthesis (2), and underlie many concepts in molecular electronics (3). The initially prepared zeroth-order state mixes with a manifold of vibronic levels of a lower electronic state, leading to the radiationless “decay” of the initial state. This decay represents a conversion of electronic to vibrational energy and is thus often the first step in the ensuing photochemical dynamics. Nonadiabatic coupling (4–8) often leads to complex, broadened absorption spectra caused by the high density of nuclear states and strong variations of transition dipole with nuclear coordinate. In some larger molecules such as pyrazine, high resolution spectroscopy can provide “exact” solutions to the study of radiationless transitions (9). In general these problems remain difficult, particularly when the state density becomes high and multi-mode vibronic couplings are involved. The case of greatest importance to photochemistry, when the zeroth-order excited states are directly or indirectly coupled to a true continuum and leading to nonadiabatic photodissociation dynamics (10, 11), is especially challenging.

Our interest is in developing time-resolved methods for the study of nonadiabatic molecular dynamics, building upon the seminal time-resolved studies of Zewail and coworkers (12). Time-resolved (or wavepacket) methods offer a complementary view of the dynamics and can yield an insightful physical picture. We begin here with a general discussion of wavepacket dynamics. Wavepackets are defined to be a coherent superposition of eigenstates. The superposition is nonstationary because of the differing energy phase factors of the eigenstates. Wavepackets can behave like zeroth-order, classical-like states and are therefore very helpful in discerning the underlying physics. The three aspects of a femtosecond pump-probe experiment are (a) the preparation or pump, (b) the dynamical evolution, and (c) the probing of the nonstationary superposition state. The amplitudes and initial phases of the set of prepared excited eigenstates are determined by the amplitude (i.e., the “spectrum”) and phase (i.e., the “temporal shape”) of the pump laser field and the transition probabilities between the ground state $|g\rangle$ and the excited state of interest. In Figure 1, we illustrate the preparation of a wavepacket by a pump pulse (black) at time $t = 0$. Once the pump laser pulse is over, the wavepacket $\chi(\Delta t)$, given by Equation 1, evolves freely according to relative energy phase factors in the superposition.

$$|\chi(\Delta t)\rangle = \sum_n \tilde{a}_n |\Psi_n\rangle e^{-i2\pi c E_n \Delta t}. \quad 1.$$

The a_n complex coefficients contain both the amplitudes and initial phases of the exact (non-BO) molecular eigenstates $|\Psi_n\rangle$, which are prepared by the pump laser $E_{\text{PUMP}}(\omega_1, t = 0)$. The E_n are the excited state eigenenergies, given here in wavenumbers. Although we show here only the case of discrete excited states, the description of a wavepacket is readily extended to include continuous states. The probe laser field interacts with the wavepacket typically after the pump pulse is over, projecting it onto a specific final state $|\Psi_f\rangle$ at some time delay Δt . This final state acts like a “movie screen” onto which the wavepacket dynamics is projected.

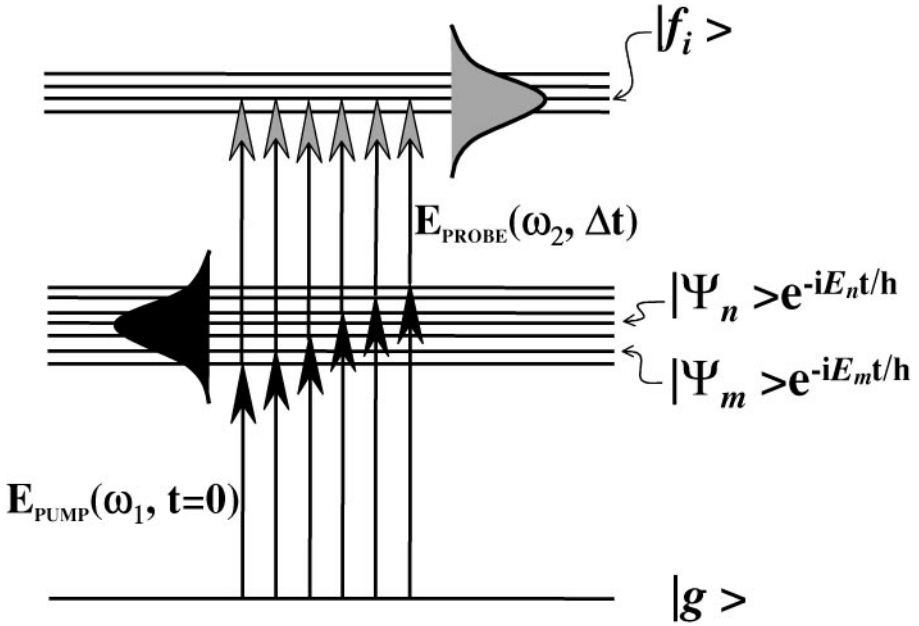


Figure 1 The creation, evolution and detection of wavepackets. The pump laser pulse E_{PUMP} (black) creates a coherent superposition state at $t=0$ from the ground state $|g\rangle$. The set of excited state eigenstates $\{|\Psi_k\rangle\}$ in the superposition (wavepacket) all have different energy phase factors, leading to nonstationary behavior (wavepacket evolution). At time Δt the wavepacket is projected by a probe pulse E_{PROBE} (grey) onto a set of final states $\{|f_i\rangle\}$, which act as a “template” for the dynamics. The time-dependent probability of being in a given final state $|f_i\rangle$ is modulated by the interferences between all degenerate coherent two-photon transition amplitudes. The choice of final state is critically important. For a discussion, see the text.

Knowing something about this movie screen and whether or not the projection is “faithful” will obviously be important. In Figure 1, we illustrate the probing of the created wavepacket by a probe pulse (grey) at time Δt . The time dependence of the differential signal, $S_i(\Delta t)$, for projection onto a single final state $|f_i\rangle$ can be thus written:

$$S_i(\Delta t) = |\langle \Psi_f | \vec{\mu}(\vec{r}) \cdot \vec{E} | \chi(\Delta t) \rangle|^2 = \left| \sum_n \tilde{b}_n e^{-i2\pi c E_n \Delta t} \right|^2, \quad 2.$$

where

$$\tilde{b}_n = \tilde{a}_n \langle \Psi_f | \vec{\mu}(\vec{r}) \cdot \vec{E}_{\text{PROBE}}(\omega_2, \Delta t) | \Psi_n \rangle$$

$$S_i(\Delta t) = \sum_n \sum_{m \leq n} |\tilde{b}_n| |\tilde{b}_m| \cos \{ (E_n - E_m) 2\pi c \Delta t + \Phi_{nm} \}.$$

The complex coefficients b_n contain the a_n from Equation 1 as well as the probe transition dipole moment and generalized vibronic overlap factors to the final state $|\Psi_f\rangle$. The most detailed information is in this final state differential signal $S_i(\Delta t)$. It arises from a coherent sum over all two-photon transition amplitudes consistent with the pump and probe laser bandwidths and therefore implicitly contains interferences between degenerate two-photon transitions. It can be seen that the signal as a function of Δt contains modulations at frequencies $(E_n - E_m)$, the set of level spacings in the superposition. It is the interference between individual two-photon transitions arising from an initial state, through different excited eigenstates and terminating in the same single final state that leads to these modulations. It is, in essence, a multi-level quantum beat. The power spectrum of this time domain signal is comprised of frequencies and amplitudes (i.e., modulation depths) that give information about the set of level spacings in the problem and their respective overlaps with a specific, chosen final state $|f_j\rangle$. Different final states $|f_j\rangle$ will generally have differing overlaps with the wavepacket leading to differing amplitudes in the power spectrum (because of differing modulation depths in the time domain signal). In general, there is often a set of final states $|\Psi_f\rangle$ (or $|f_i\rangle$) that may fall within the probe laser bandwidth. We must differentiate, therefore, between integral and differential detection techniques. With integral detection techniques (e.g., total fluorescence, total ion yield), the experimentally measured total signal, $S(\Delta t)$, is proportional to the total population in the final states, $\Sigma S_i(\Delta t)$, created at the end of the two-pulse sequence. It can be seen that information is lost in carrying out the sum $\Sigma S_i(\Delta t)$ since the different final states $|f_i\rangle$ may each have different overlaps with the wavepacket. Therefore, differential techniques (e.g., dispersed fluorescence, photoelectron spectroscopy), which can disperse the observed signal with respect to final state $|f_i\rangle$, will be important. Clearly the choice of the final state is of great importance as it determines the experimental technique and significantly determines the information content of an experiment. In many studies of nonadiabatic processes in polyatomic molecules, the initially prepared “bright” state is often coupled to a lower-lying “dark” state. The fact that this latter state is dark means that observation of its dynamics is potentially obscured, depending greatly upon the nature of the final state.

The particular choice of the molecular ionization continuum as the final state $|\Psi_f\rangle$ in polyatomic wavepacket experiments has both practical and conceptual advantages (13, 14): (a) Charged particle detection is extremely sensitive. (b) Detection of the ion provides mass information on the carrier of the spectrum. (c) Ionization is always an allowed process, with relaxed selection rules owing to the range of symmetries of the outgoing electron. Any molecular state can be ionized. There are no dark states in photoionization. (d) Highly detailed, multiplexed information can be obtained by differentially analyzing the outgoing photoelectron as to its kinetic energy (15–23) and angular distribution (24–30). The TRPES technique has been demonstrated to be quantitatively accurate in providing direct measurements of electronic relaxation rates (31). Zero electron kinetic energy-pulsed field ionization (ZEKE-PFI) detection (32) can be used for high

sensitivity, state specific detection (13, 14, 33–35). (e) Higher order (multiphoton) processes, which can be very difficult to avoid in femtosecond experiments, are readily revealed. (f) Photoelectron-photoion coincidence measurements can allow for studies of cluster solvation effects as a function of cluster size and for studies of vector correlations in photodissociation dynamics.

Time-resolved photoelectron spectroscopy (TRPES) has been recently reviewed (36) and we refer the reader there for a discussion of the historical development of the field. In this review (see also 37), we concentrate on physical concepts and illustrations of its applicability to problems in nonadiabatic molecular dynamics. Photoelectron spectroscopy is particularly well suited to nonadiabatic coupling problems because it is sensitive to both electronic configurations and vibrational dynamics (38). An elementary but useful picture is that emission of an independent outer valence electron occurs without simultaneous electronic reorganization of the ion core (the “molecular orbital” or Koopmans’ picture). These simple correlation rules indicate the cation state expected to be formed upon single photon, single active electron ionization of a given molecular orbital. Partial ionization probabilities into specific cation electronic states can differ drastically with respect to the molecular orbital nature of the neutral electronic state. If a given neutral electronic configuration correlates—upon removal of a single active outer valence electron—to the ground electronic configuration of the cation, then the photoionization probability is generally higher than if it does not. This suggests the possibility of using the electronic structure of the cation as a probe of nonadiabatically evolving electronic configurations in the neutral excited state.

In Figure 2, we show a picture of excited state polyatomic wavepacket dynamics probed via TRPES. A zeroth-order bright state α is coherently prepared with a femtosecond pump pulse. According to the Koopmans’ picture, it should ionize into the α^+ continuum, the electronic state of the cation obtained upon removal of the outermost valence electron (here chosen to be the ground electronic state of the ion). This process produces a photoelectron band ε_1 . We now consider any nonadiabatic coupling process that transforms the zeroth-order bright state α into a lower lying zeroth-order dark state β , as induced by promoting vibrational modes of appropriate symmetry. Again, according to the Koopmans’ picture, the β state should ionize into the β^+ ionization continuum (here assumed to be an electronically excited state of the ion), producing a photoelectron band ε_2 . Therefore, for a sufficiently energetic probe photon (i.e., with both ionization channels open), we expect a switching of the electronic photoionization channel from ε_1 to ε_2 during the nonadiabatic process. This simple picture suggests that one can monitor directly the evolving excited state electronic configurations (i.e., the electronic population dynamics) during nonadiabatic processes while simultaneously following the coupled nuclear dynamics via the vibrational structure within each photoelectron band. In other words, the electronic structure of the molecular ionization continuum acts as a “template” for the disentangling of electronic from vibrational dynamics in the excited state. This disentangling via TRPES was demonstrated in a study of nonadiabatic dynamics in a linear polyene (23).

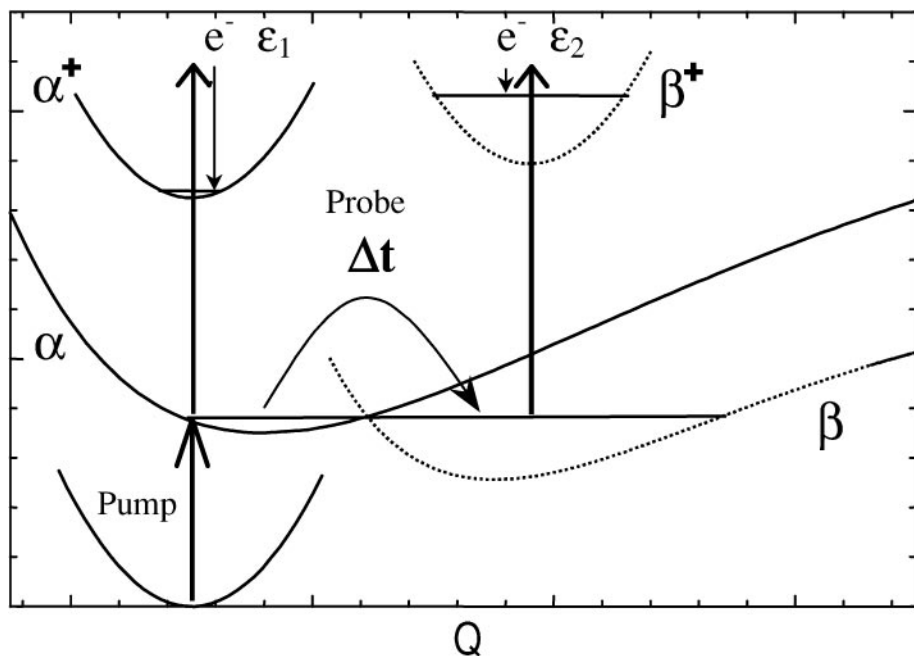


Figure 2 A TRPES scheme for disentangling electronic from vibrational dynamics in excited polyatomic molecules. A zeroth-order electronic state α is prepared by a fs pump pulse. Via a nonadiabatic process, it converts to a vibrationally hot lower lying electronic state, β . The Koopmans'-type ionization correlations suggest that these two states will ionize into different electronic continua: $\alpha \rightarrow \alpha^+ + e^- (\epsilon_1)$ and $\beta \rightarrow \beta^+ + e^- (\epsilon_2)$. When the wavepacket has zeroth-order α character, any vibrational dynamics in the α state will be reflected in the structure of the ϵ_1 photoelectron band. After the nonadiabatic process, the wavepacket has β zeroth-order electronic character, and any vibrational dynamics in the β state will be reflected in the ϵ_2 band. This allows for the simultaneous monitoring of both electronic and vibrational excited state dynamics, as discussed in the text.

The other component of the molecular ionization continuum final state is the free electron. The symmetries of the outgoing electron partial waves are likewise related to the symmetry of the electronic state undergoing ionization. This can be viewed most simply (Equation 3) as caused by the requirement that the product of the symmetry species of the prepared excited state Γ_{ex} , the dipole operator Γ_{μ} , the ion state Γ_+ , and the free electron wavefunction Γ_{e^-} must contain the totally symmetric irreducible representation Γ_{TS} of the molecular symmetry group, in order that the transition be allowed.

$$\Gamma_{\text{ex}} \otimes \Gamma_{\mu} \otimes \Gamma_+ \otimes \Gamma_{e^-} \supseteq \Gamma_{\text{TS}}. \quad 3.$$

It can be seen that if, because of a nonadiabatic process, the symmetry species of the initial zeroth-order state Γ_{ex} changes, then the symmetry species of the

outgoing electron Γ_{e^-} must also change in order that the product remain (or contain) the totally symmetric species Γ_{TS} . It is the symmetry species of the outgoing electron Γ_{e^-} that relates to the photoelectron angular distribution. Hence, measurement of time-resolved photoelectron angular distributions (PADs) also provide a probe of electronically nonadiabatic processes. The use of time-resolved PADs in excited-state molecular dynamics has been recently reviewed, and we refer the reader to these for detailed discussions (39–41). The measurement of time-resolved PADs is expected to be particularly valuable when dynamical processes are not discernable from a photoelectron kinetic energy analysis alone. In general, PADs measurements are more involved and their calculation much more challenging in polyatomic systems than for the case of photoelectron energy distributions. A consideration of “practical” issues such as the nature of the lab-frame alignment (i.e., how the pump pulse creates an anisotropic distribution of excited state axes in the lab-frame) is important. Unfavorable lab-frame alignment can potentially obscure the underlying photoionization dynamics and reduce the efficacy of the PAD as an experimental probe of electronic nonadiabaticity. This unfortunate circumstance has been observed, for example, in a femtosecond time-resolved PADs study of phenanthrene internal conversion, despite the fact that symmetry arguments indicate that the PADs from ionization of each of the coupled electronic states (in this case, S_2 and S_1) contain different partial waves (J.P. Shaffer, A.M.D. Lee, M. Schmitt, A. Stolow, C.C. Hayden, personal communication).

Photoionization always produces two species available for analysis—the ion and the electron. The extension of the photoelectron-photoion-coincidence (PEPICO) technique to the femtosecond time-resolved domain has been demonstrated and shown to be useful for studies of dynamics in clusters (43). Time and angle-resolved PEPICO measurements yielding ion-electron kinetic energy and angular correlations will shed new light on photodissociation dynamics in polyatomic molecules. Correlated photofragment and photoelectron velocities can provide a complete probe of the dissociation process (44, 45). The photofragment recoil measurement defines the energetics of the dissociation process and the alignment of the recoil axis in the lab frame, the photoelectron energy provides spectroscopic identification of the products, and the photoelectron angular distribution can be transformed to the recoil frame in order to extract vector correlations such as the photofragment angular momentum polarization. The integration of photoion-photoelectron energy and angular correlation measurements with femtosecond laser technology was demonstrated by Hayden and coworkers at Sandia National Labs and allows the time evolution of complex dissociation processes to be studied (46).

The subsequent sections of this paper are arranged as follows. We shall discuss experimental aspects of femtosecond TRPES, describing our laser system and give examples using both zero-kinetic energy (ZEKE) and magnetic bottle time-of-flight techniques. Detailed diatomic wavepacket dynamics are discussed and interpreted. The use of the molecular ionization continuum as a final state in polyatomic studies is discussed in more detail and the two limiting cases of Koopmans’ correlations are presented, along with experimental examples of each case. The

applications of TRPES to molecular dynamics are in our opinion manifold and we present specific examples in the areas of excited state intramolecular proton transfer, photoisomerization dynamics, and nonadiabatic photodissociation dynamics.

EXPERIMENTAL METHODS

Femtosecond Laser Technology

The progress in femtosecond TRPES over the past ten years derives from prior developments in femtosecond laser technology, because techniques for photoelectron spectroscopy have been highly developed for some time. Experimental aspects of femtosecond TRPES are discussed in more detail elsewhere (47). In Figure 3, we show a schematic layout of the present NRC femtosecond laser system. A fs Ti:Sapphire oscillator (Spectra-Physics Tsunami) and a ps Nd:YAG oscillator (Lightwave Electronics 131) are each electronically locked (via phase-locked loops) to a stabilized 80 MHz external reference oscillator (Wiltron 68147B). This synchronizes the optical pulse trains from the two oscillators to within 1–2 ps. The Ti:Sapphire oscillator is pumped by a diode-pumped Nd:YVO₄ laser (Spectra Physics Millennia). The ps Nd:YAG oscillator is directly diode-pumped. The ~80 fs, 800 nm Ti:Sapphire pulses are stretched to a few hundred ps and then regeneratively amplified (Positive Light, Spitfire) using a 10 mJ, 1 kHz Nd:YLF laser (Positive Light, Evolution30) as the pump source. These pulses then pass through a linear Ti:Sapphire amplifier, pumped by a 12 mJ, 1 kHz Nd:YLF laser (Positive Light, Evolution30). This yields ~4 mJ/pulse at 1 kHz. Upon compression, about 2.75 mJ, 80 fs pulses at 1 kHz are obtainable. The 150 ps 1064 nm pulses from the Nd:YAG oscillator can be amplified to ~1.5 mJ/pulse in a NRC-design (48) 1 kHz diode-pumped Nd:YVO₄ grazing incidence slab laser (GISL). This synchronized, amplified ps laser and its harmonics are used for many purposes.

The amplified Ti:Sapphire output is used to pump several OPAs. High power pulses at 800 nm pump two OPAs (Quantronix Light Conversion, TOPAS), each producing 60–100 fs pulses continuously tunable within the range of 1200–2600 nm. These can each be doubled or sum-mixed with the pump and subsequently doubled or sum-mixed again to produce tunable fs UV pulses. Second harmonic generation of the amplified Ti:Sapphire laser yields 400 nm pulses that are used to pump two noncollinear OPAs (Clark-MXR NOPA). These produce very short (15–20 fs) pulses with a few μJ of energy, continuously tunable in the range of 480–750 nm. A computer controlled stepper motor is used to control the time delay between the pump and probe laser systems.

Photoelectron Spectroscopy

Spectrometers for femtosecond TRPES have modest requirements as compared to modern standards for photoelectron spectrometers. The bandwidth (FWHM) of a Gaussian 50 fs pulse is $\sim 300 \text{ cm}^{-1}$. A pump-probe measurement involves the convolution of two such pulses, leading to an effective bandwidth of $\sim 50 \text{ meV}$.

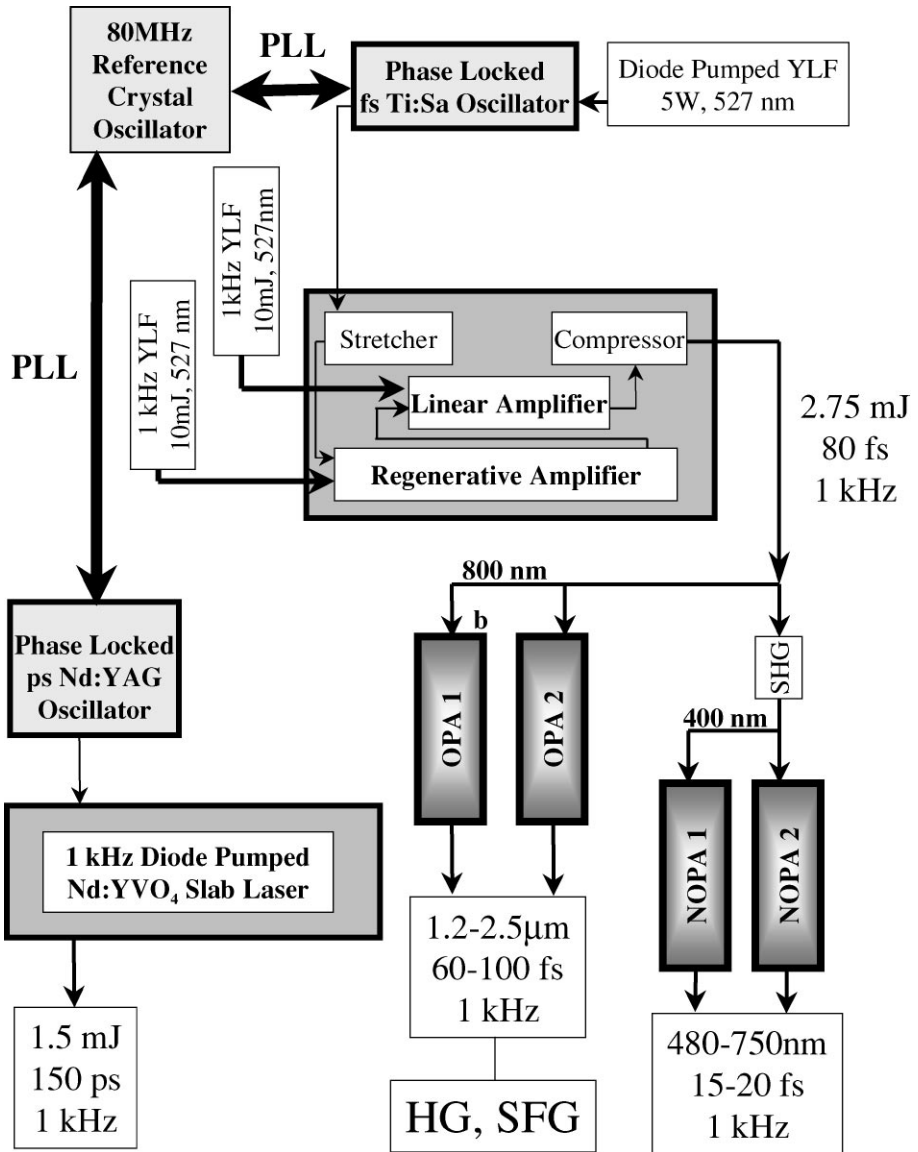


Figure 3 The NRC Femtosecond Laser System. fs Ti:Sapphire and ps Nd:YAG oscillators are electronically synchronized (PLL) and each amplified at 1 kHz. The Ti:Sapphire pulse is stretched, regeneratively amplified, linearly amplified and subsequently compressed for output (2.75 mJ, 80 fs). The ps YAG pulses are amplified in a NRC-design diode-pumped Nd:YVO₄ cavity (1.5 mJ, 150 ps). The amplified Ti:Sapphire output at 800 nm is used to pump two multi-pass OPAs (OPA1, OPA2), producing fs near-IR tunable pulses. 400 nm pulses from second harmonic generation of the Ti:Sapphire output are used to pump two noncollinear OPAs (NOPA1, NOPA2), producing broadly tunable, very short (~15 fs) pulses throughout the visible region. For a detailed discussion, see the text.

This limits the energy resolution required in measuring the energy of the photoelectrons.

In zero-electron kinetic energy (ZEKE) photoelectron spectroscopy the probe pulse does not directly ionize the molecules excited by the pump pulse but rather excites them to a manifold of high lying Rydberg states (32). After a time interval (typically 1 μ s) to allow kinetic electrons to leave the ionization region, a pulsed electric field of typically 0.5–1 V/cm ionizes the high Rydberg states and accelerates them toward a detector. The technique provides essentially unit collection efficiency for the ZEKE electrons and hence very high signal-to-noise ratios are obtained. A drawback of the ZEKE method is that the probe laser must be tuned if the complete photoelectron spectrum need be recorded. By contrast, electron time-of-flight methods do not usually require tuning of the laser. These methods, however, generally suffer from much lower signal-to-noise ratios.

An improvement in electron time-of-flight collection efficiency while retaining the advantages of the time-of-flight measurement can be obtained by using a magnetic bottle spectrometer (49), as shown in Figure 4 and discussed in more detail elsewhere (47). We emphasize that in fs pump-probe experiments, the laser intensity must be kept below multiphoton ionization thresholds. This simply requires a reduction of the laser intensity until one-photon processes dominate. In order to recover acceptable signal levels, the target density must be increased. Hence, we implement a high intensity molecular beam source, as shown in Figure 4. The source chamber has $\sim 10,000$ l/s pumping speed—four large diffusion pumps (Edwards EO250) backed by a Roots blower. A doubly skimmed beam passes through the main interaction chamber, which is differentially pumped by a 400 l/s “maglev” turbo (Seiko Seiki STP400C). The electron time-of-flight tube is differentially pumped by another 400 l/s “maglev” turbo (Seiko Seiki STP400). This photoelectron spectrometer has a base pressure of 2×10^{-10} torr and is kept warm (typically 80°C) in order to minimize changes in surface electric potentials during experiments.

Amplified femtosecond laser pulses are inherently intense, and experimentalists and theorists alike must be cognizant of this. The neglect of intensity effects can lead to misinterpretation of results. Even moderate focussing ($f/40$) of a 100 fs pulse (at $\lambda = 300$ nm) yields an intensity of 10^{12} W/cm² with a pulse energy of only 1 μ J! It can be seen that amplified femtosecond pulse experiments will be very difficult to carry out in the perturbation theory (Golden rule) limit of, say, 10^6 – 10^8 W/cm². As the strong laser field physics of molecules is amply discussed elsewhere (50), we summarize here only briefly some potential consequences of the nonperturbative fields that can appear in almost any femtosecond experiment using amplified pulses. For example, strong Rabi oscillations can lead to aligned states and to ground state wavepackets. Another important consequence of nonperturbative intensities is the AC Stark effect—the shifting and modification of potential energy surfaces during the strong electric field of the laser pulse. This leads to an alteration of the molecular dynamical evolution and to sweeping field-induced resonances that may introduce phase-shifts in the probe laser signal. From

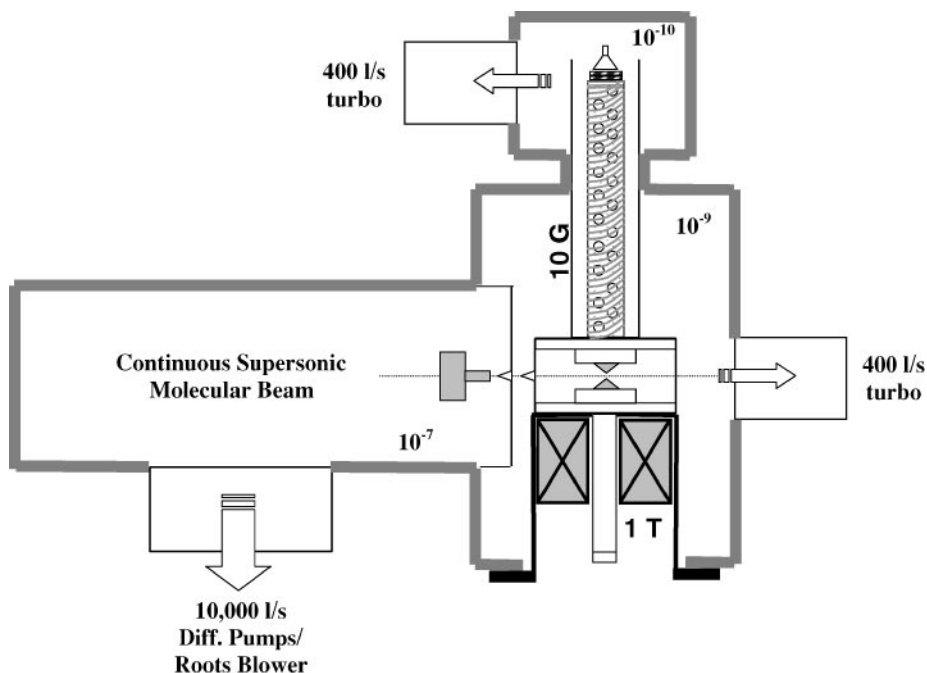


Figure 4 The NRC magnetic bottle photoelectron spectrometer. The bottle uses a 1 Tesla parallelizing field that leads into a 10 Gauss guiding field in the electron drift tube. The geometry is optimized for high intensity molecular beam throughput. The diffusion-pumped source chamber (10^4 l/s) houses a continuous variable temperature molecular beam nozzle. The molecular beam is doubly skimmed before passing through the magnet pole pieces (1 T). The interaction chamber and electron drift tube are each pumped by a 400 l/s turbo pump. The base pressure of the spectrometer is 10^{-10} torr. For a detailed discussion, see the text.

a very practical point of view, it is often difficult to use one-photon preparation of an excited state wavepacket unless the absorption cross-section for this step is large. The reason for this is that femtosecond pulses generally favor nonlinear over linear processes. The only solution is to reduce the laser intensity (W/cm^2) until the one-photon process dominates. The signal levels at this point, however, may be very small and sensitive detection techniques will be required.

In the ionization continuum, the AC Stark effect manifests itself in terms of the ponderomotive potential U_p , well known in strong field atomic physics (51). Classically, the ponderomotive potential of an electron in a laser field of strength E and frequency ω is given by the time-averaged “wiggling” energy:

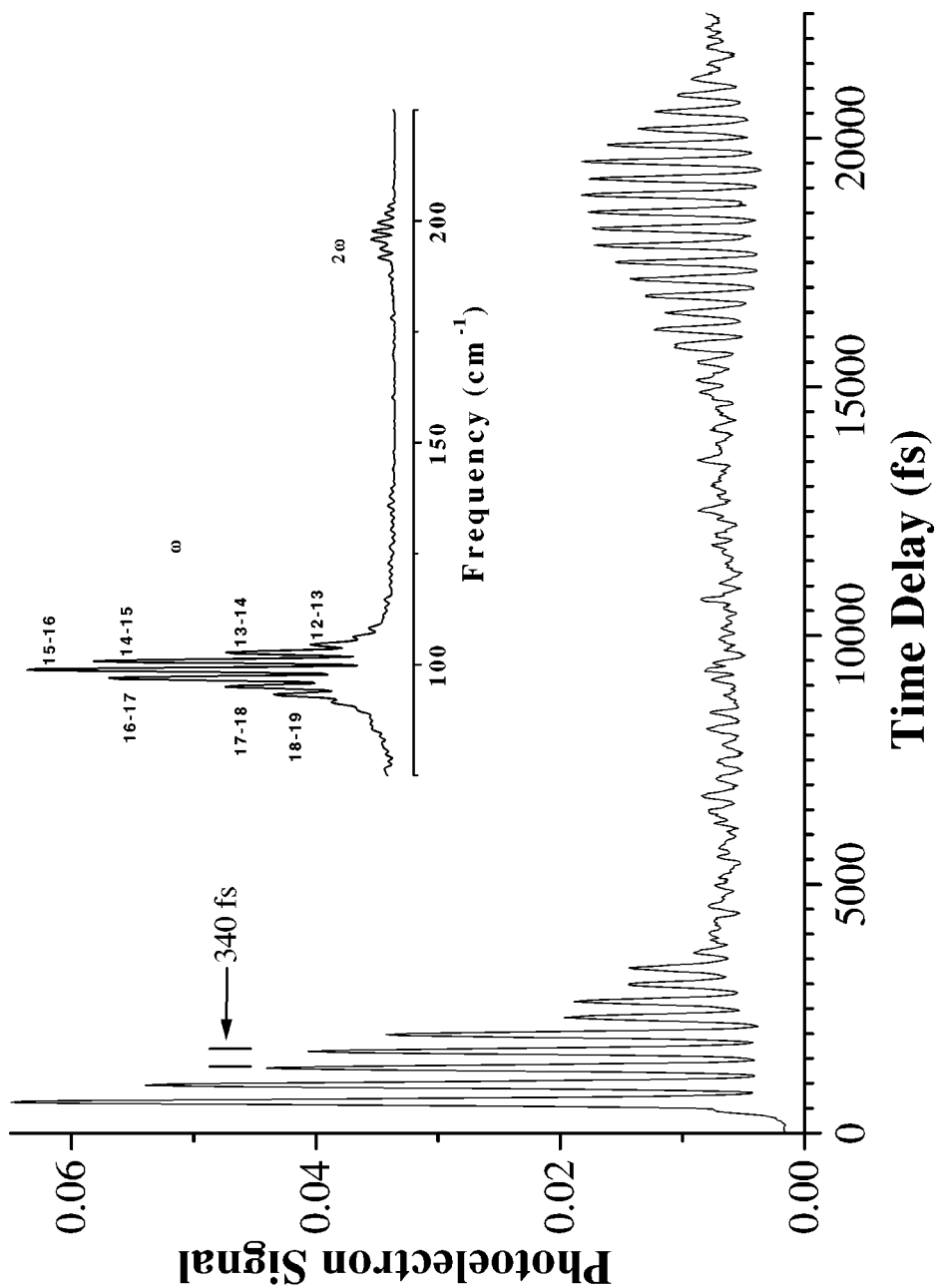
$$U_p = \frac{e^2 E^2}{4m_e \omega^2}. \quad 4.$$

A convenient rule of thumb is that the ponderomotive shift is 10 meV per TW/cm² at 330 nm. U_p scales linearly with laser intensity and quadratically with wavelength. Because of the spatio-temporal averaging of intensities in the pulse, the ponderomotive effect is observed as a blue shift and broadening of the photoelectron spectrum (52).

WAVEPACKET DYNAMICS

In order to gain further insight into wavepacket dynamics and its applications (53), we believe it is useful to begin with the case of a diatomic molecule. Here we discuss I₂ (B) vibrational wavepacket dynamics and the use of time-resolved ZEKE photoelectron detection, as shown in Figure 5 (13, 14). In this experiment, a femtosecond pump pulse at 580 nm prepared a vibrational wavepacket in the B-state. The classical-like state formed in this way is expected to oscillate back and forth in the molecular potential at its classical frequency of oscillation (in this case, 340 fs). As a function of time delay, a two-photon probe at 345 nm projected this wavepacket onto the ground vibrational state of the ion. After a time delay of 1 μ s in which all free electrons escaped, a 2 V/cm pulsed field ionized the high-lying Rydberg states and pushed the ZEKE-PFI electrons toward the detector. The collected ZEKE electron signal, plotted in Figure 5, oscillates as a function of time delay. This temporal modulation directly reflects the wavepacket vibrational motion in the B-state potential with a period of 340 fs. As the vibrational states dephase, the classical-like oscillation disappears around 3–4 ps. Eventually, the eigenstates recover their initial phases and the wavepacket revives (54), in this case around 18 ps. In the frequency domain picture, these temporal modulations are caused by interferences between the individual transitions from different B-state eigenstates terminating in the same final ionic state and are described by nearest-neighbor coherences as well as higher-order coherences (see Figure 1). As discussed in the Introduction, the power Fourier transform of this time-domain data, inset in Figure 5, reveals the set of vibrational level spacings (e.g., $\nu = 15/\nu = 16$ etc.) responsible for the time-domain signal. These results also

Figure 5 Femtosecond time-resolved ZEKE photoelectron spectroscopy of vibrational wavepacket dynamics in a diatomic molecule, I₂ (B). Well resolved 340 fs modulations can be seen, corresponding to classical-like vibrational motion in the excited B-state. The wavepacket undergoes quantum mechanical dephasing in \sim 3–4 ps, indicating a loss of classical localization. The wavepacket remains fully coherent and exhibits a full revival at \sim 18 ps, when the classical localization returns. Inset is the power Fourier transform of this time domain data, showing the B-state vibrational coherences (ω for first order, around 100 cm⁻¹; 2ω for second order, around 200 cm⁻¹) responsible for the time domain signal, as discussed in the text. Very high signal-to-noise ratios are obtainable with the ZEKE technique.



show the high, background-free signal-to-noise ratios obtainable with ZEKE detection.

DISENTANGLING ELECTRONIC FROM VIBRATIONAL DYNAMICS

The simple Koopmans' picture suggests that one might be able to directly monitor the evolving excited state electronic configurations during nonadiabatic processes while simultaneously following the coupled nuclear dynamics via the vibrational structure within each photoelectron band. This "disentangling" of electronic from vibrational dynamics during nonadiabatic processes gives a new view of excited polyatomic molecules (23).

We have discussed the two limiting cases for Koopmans'-type correlations in such experiments (55, 56). The first case, Type (1), is when the neutral excited states α and β clearly correlate to different ion electronic continua, as suggested in Figure 2. Even if there are large geometry changes upon internal conversion and/or ionization, producing long vibrational progressions, the electronic correlations should favor a disentangling of the vibrational dynamics from the electronic population dynamics, as discussed in detail elsewhere (55). Type (1) systems are found, for example, in the photodynamics of linear polyenes and, below, we discuss the specific example of *all-trans* decatetraene. The other limiting case, Type (2), is when the neutral excited states α and β correlate equally strongly to the same ion electronic continua. This is expected to hinder the disentangling of electronic from vibrational dynamics, as discussed in detail elsewhere (56). Type (2) systems are found, for example, in the photodynamics of polyaromatic hydrocarbons and, below, we discuss the specific example of phenanthrene.

Type (1): Complementary Koopmans'-Type Correlations

As an example of Type (1) correlations, we consider ultrafast internal conversion in the linear polyene *all-trans* 2,4,6,8 decatetraene (DT). The investigation of polyene photophysics is central to our understanding of electron delocalization and electron correlation in molecules. They have also been a test bench for quantum chemical theory owing to their lowest excited state containing doubly excited configurations (57). The first optically allowed transition in DT is $(S_2)1^1B_u \leftarrow (S_0)1^1A_g$. The S_2 state is a singly excited configuration. The lowest excited state is the dipole forbidden $(S_1)2^1A_g$ state, which arises from configuration interaction between singly and doubly excited A_g configurations. Nonadiabatic coupling leading to ultrafast internal conversion from S_2 to S_1 is promoted by b_u symmetry vibrational motions. DT provides a classic example of internal conversion in a polyene (58), making it a good candidate for testing our method. As discussed in detail elsewhere (55), the S_2 excited state electronically correlates with the $(D_0) 1^2B_g$ ground electronic state of the cation. The S_1 state, by contrast, correlates predominately with the $(D_1) 1^2A_u$ first excited state of the cation and DT, therefore, is a Type (1) molecule.

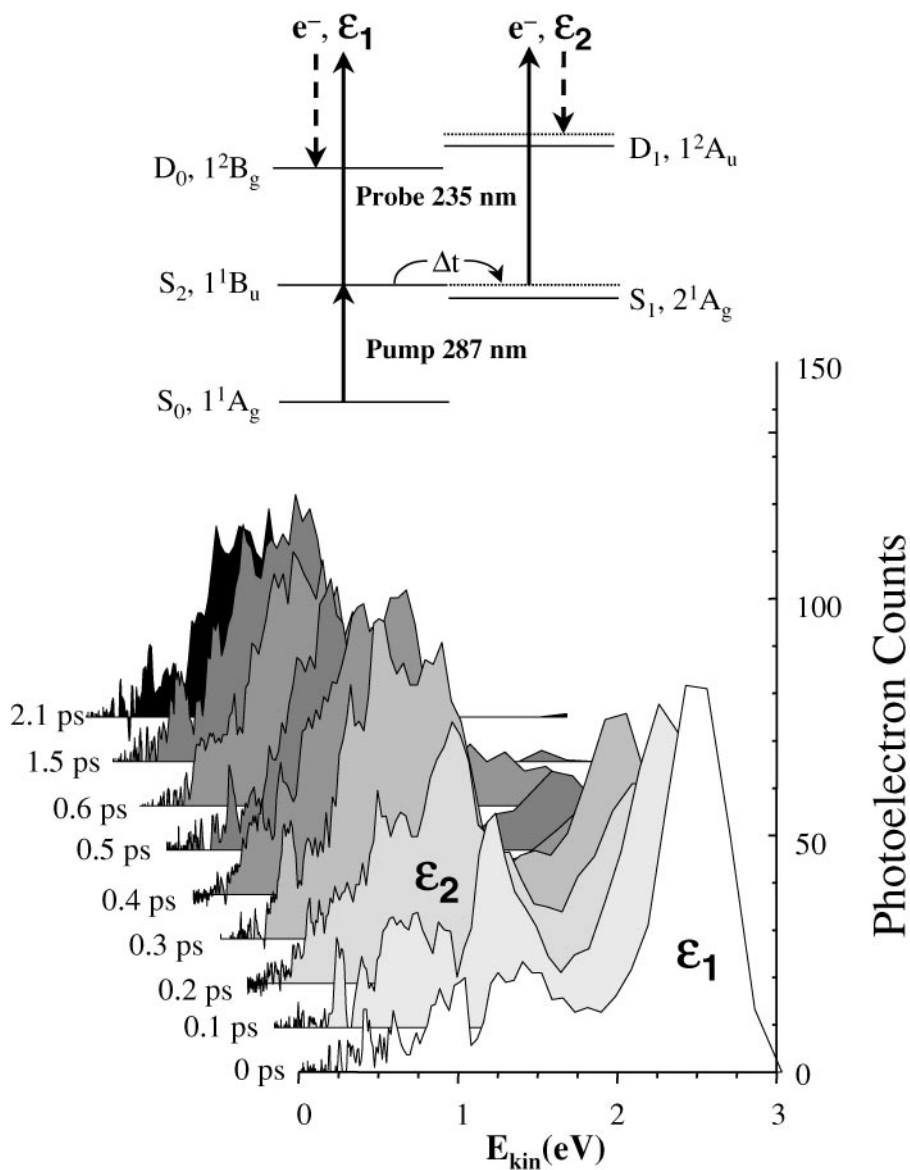
In Figure 6 (top) we show the energy level scheme relevant to the DT experiment. A femtosecond pump pulse at 287 nm (4.32 eV) prepared the excited S_2 state at its vibrationless electronic origin. It then evolves into a vibrationally hot (~ 0.7 eV) S_1 electronic state via internal conversion. The idea is to observe the rapidly evolving electronic states by projecting the wavepacket onto several cation electronic states using a UV probe photon of sufficient energy (here, 235 nm, 5.27 eV). As the nonadiabatic coupling proceeds, the evolving electronic character of the wavepacket alters the photoionization electronic channel, leading to large shifts in the time-resolved photoelectron spectrum. The experimental photoelectron kinetic energy spectra in Figure 6 (bottom) are characterized by a rapid shift of electrons from an energetic component ($\varepsilon_1 = 2.5$ eV) to a broad, structured low energy component (ε_2). This shift is the direct (as opposed to inferred) signature of the changing electronic state induced by nonadiabatic coupling. The 2.5 eV band is owing to ionization of S_2 into the D_0 ion state. The broad, low-energy band arises from photoionization of S_1 , which correlates with the D_1 ion state. Its appearance is caused by population of the S_1 state via internal conversion. Integration of the two photoelectron bands directly reveals the S_2 to S_1 internal conversion timescale of 386 ± 65 fs. It is important to note that these results contain more information than the overall (integrated) internal conversion time. The vibrational structure in each photoelectron band yields information about the vibrational dynamics that promote and tune the electronic population transfer. In addition, it gives a direct view of the evolution of the ensuing intramolecular vibrational energy redistribution (IVR) in the “hot molecule” that occurs on the dark S_1 potential surface. This Type (1) example of DT demonstrates the selectivity of the molecular ionization continuum for specific neutral configurations. Furthermore, it shows that for favorable Koopmans'-type correlations, the electronic population dynamics can indeed be disentangled from the vibrational dynamics (23, 55).

Type (2): Corresponding Koopmans'-Type Correlations

We now consider Type (2) systems in which the one-electron correlations upon ionization lead to the same cationic states. In this case, we would not expect such a favorable separation of electronic from vibrational dynamics, as was seen for the Type (1) example of DT. Examples of Type (2) systems include the polyaromatic hydrocarbons, and here we consider the specific example of S_2 - S_1 internal conversion in phenanthrene (PH), discussed in detail elsewhere (56). In the case of PH, both the S_2 and the S_1 states correlate similarly with the electronic ground state as well as the first excited state of the cation.

In PH, the nonadiabatic coupling of the bright electronic state (S_2) with the dense manifold of zeroth-order S_1 vibronic levels leads to the nonradiative decay (dephasing) of the zeroth-order S_2 state. The energy gap between these two excited states is large and the density of S_1 vibronic levels is extremely large compared to the reciprocal electronic energy spacing. The dark state forms an apparently smooth quasicontinuum. Such a situation is known as the statistical limit for the

radiationless transition problem and PH provides an example of this (56). The very small and unequal level spacings in the problem mean that the revival time of the initially prepared state may be very long compared to other timescales, and therefore the dephasing of the initially prepared zeroth-order state may appear irreversible. The statistical limit is phenomenologically characterized by Lorentzian



absorption bands where the apparent homogeneous width Γ is related to the apparent “lifetime” of the bright state, $\tau \sim \hbar/\Gamma$.

As illustrated in Figure 7 (top), we excited PH from the S_0 1A_1 ground state to the origin of the S_2 1B_2 state with a 282 nm (4.37 eV) fs pump pulse. The excited molecules are then ionized after a time delay Δt using a 250 nm (4.96 eV) probe photon. The S_2 1B_2 state rapidly internally converts to the lower lying S_1 1A_1 state at 3.63 eV, transforming electronic into vibrational energy. In PH, both the S_2 1B_2 and S_1 1A_1 states can correlate with the D_0 2B_1 ion ground state, producing the ε_1 and ε_2 photoelectron bands. With higher probe photon energies, they can also each correlate with the D_1 2A_1 ion excited state, producing other photoelectron bands (47). In Figure 7 (bottom) we show time-resolved photoelectron spectra for PH, revealing a rapidly decaying but energetically narrow peak at $\varepsilon_1 \sim 1.5$ eV. This peak is caused by photoionization of the vibrationless S_2 1B_2 state into the ionic ground state D_0 2B_1 . In order to monitor the zeroth-order S_2 electronic population decay, this time-dependent peak was integrated and plotted as a function of time, resulting in a decay-time constant of 522 ± 16 fs. This direct measurement confirms a previous result based upon rotational deconvolution of the S_2 absorption lineshape (59). The broad band, centered at about ~ 0.7 eV, in these photoelectron spectra is caused by ionization of vibrationally hot molecules in the S_1 state, formed by the S_2 – S_1 internal conversion. At times $t > 1500$ fs or so (i.e., after internal conversion), the photoelectron spectrum is comprised exclusively of signals caused by S_1 ionization. The S_1 state itself is long lived on the timescale of the experiment. Despite the fact that Type (2) molecules present an unfavorable case for disentangling electronic from vibrational dynamics, we can still see in PH a dramatic shift in the photoelectron spectrum as a function of time. This is caused by the fact that PH is a rigid molecule and the S_2 , S_1 , and D_0 states all have similar geometries. The photoionization probabilities are therefore expected to be dominated by small Δv transitions. Hence, the 0.74 eV vibrational energy in the populated S_1 state should be roughly conserved upon ionization into the D_0 ionic state. That is to say, we would expect the edge of the ε_2 band to be shifted to lower

←

Figure 6 (Top) Energy level scheme for TRPES of all-trans decatetratene, an example of a Type (1) molecule. The pump laser prepares the optically bright state S_2 . Upon ultrafast internal conversion, this state converts to the lower lying state S_1 with ~ 0.7 eV of vibrational energy. The expected complementary Type (1) Koopmans’ correlations are shown: $S_2 \rightarrow D_0 + e^-(\varepsilon_1)$ and $S_1 \rightarrow D_1 + e^-(\varepsilon_2)$. (Bottom) TRPES spectra of DT pumped at 287 nm and probed at 235 nm. There is a rapid shift (~ 400 fs) from ε_1 , an energetic band at 2.5 eV caused by photoionization of S_2 into the D_0 cation ground electronic state, to ε_2 a broad, structured band at lower energies because of photoionization of vibrationally hot S_1 into the D_1 cation first excited electronic state. The structure in the low-energy band reflects the vibrational dynamics in S_1 . These results illustrate the disentangling of the vibrational from the electronic population dynamics, as discussed in the text.

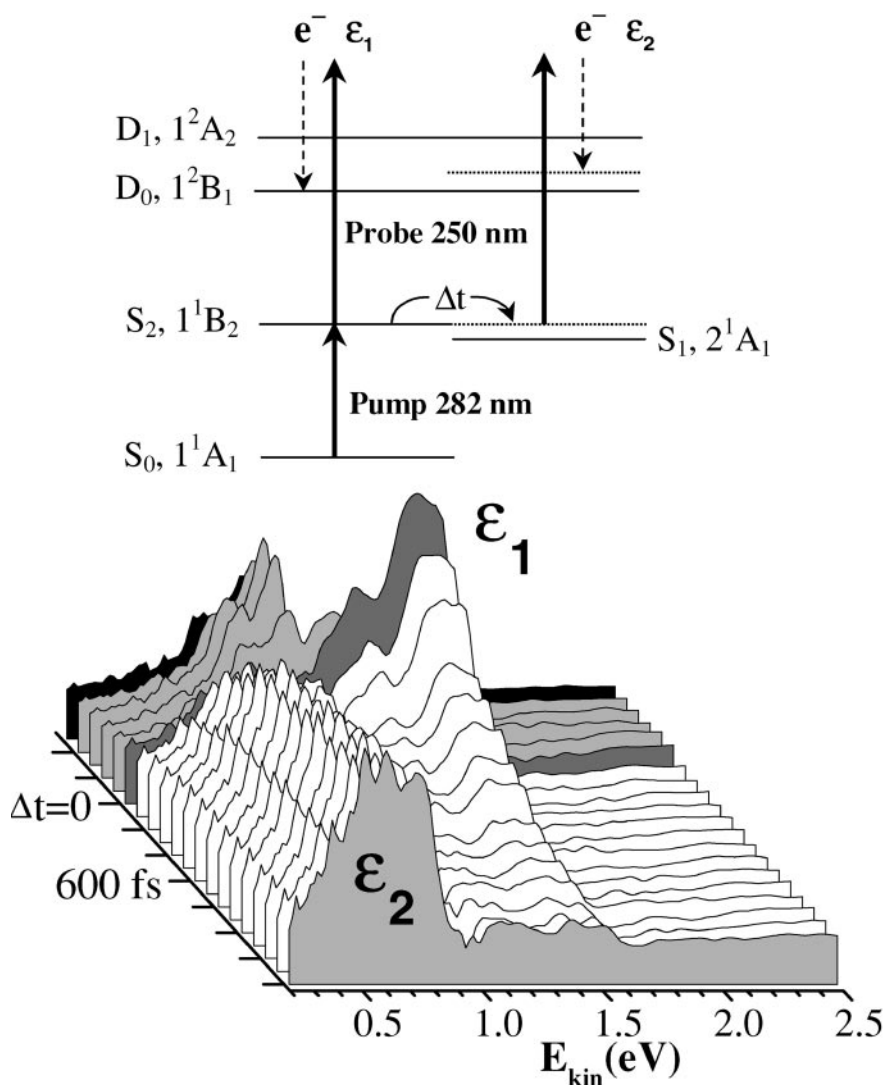


Figure 7 (Top) Energy level scheme for TRPES of phenanthrene, an example of a Type (2) molecule. The pump laser prepares the optically bright state S_2 . Ultrafast internal conversion converts this state to the lower lying state S_1 , with ~ 0.74 eV of vibrational energy. The expected corresponding Type (2) Koopmans' correlations are shown: $S_2 \rightarrow D_0 + e^-(\epsilon_1)$ and $S_1 \rightarrow D_0 + e^-(\epsilon_2)$. (Bottom) TRPES spectra of phenanthrene for a pump wavelength of 282 nm and a probe wavelength of 250 nm. The disappearance of band ϵ_1 at ~ 1.5 eV and growth of band at ϵ_2 at ~ 0.5 eV represents a direct measure of the S_2 - S_1 internal conversion time (520 fs). Despite the unfavorable Type (2) correlation, the rigidity of this molecule allows for direct observation of the internal conversion via vibrational propensities alone. For a discussion, see the text.

energies by about 0.75 eV as compared with the ε_1 band. Indeed this is what is observed. Therefore, for PH, small geometry changes favor conservation of vibrational energy upon ionization and thereby permit the observation of the excited state electronic population dynamics via a photoelectron kinetic energy analysis alone. In general, however, significant geometry changes will lead to overlapping photoelectron bands, hindering the disentangling of vibrational from electronic dynamics.

Applications

In other examples of applications in molecular dynamics, we investigated the suitability of TRPES to the study of substituent effects in molecular electronic relaxation dynamics using a series of monosubstituted benzenes as model compounds (31). Three basic types of electronic substituents were used: C=C (styrene), C=O (benzaldehyde), and C \equiv C (phenylacetylene). In addition, the effects of the rigidity and vibrational density of states of the substituent were investigated via both methyl (α -methylstyrene and acetophenone) and alkyl ring (indene) substitution. The results fit very well with the current understanding of aromatic photophysics, demonstrating that TRPES does indeed provide for a facile, accurate, and direct means of studying electronic relaxation dynamics in a wide range of molecular systems.

As an example of using TRPES to observe vibrational effects in electronic relaxation, we have recently completed a detailed comparison of electronic relaxation rates in the linear α,β -enones: acrolein (i.e., propenal), methyl vinyl ketone (i.e., α -methyl propenal), and crotonaldehyde (i.e., γ -methyl propenal) (60; J.P. Shaffer, M. Schmitt, T. Schultz, M.Z. Zgierski, I-C. Chen, M. Olivucci, A. Stolow, unpublished manuscript). Very dramatic effects on the electronic relaxation rates caused by the location of the methyl group were observed: upon S_2 ($\pi\pi^*$) excitation, crotonaldehyde relaxed \sim five times more rapidly than either methyl vinyl ketone or acrolein. The identical number of degrees of freedom in methyl vinyl ketone and crotonaldehyde suggest that vibrational density of states is not the dominant effect. The methyl effect on the torsional conical intersections could be caused by a change in diabatic versus adiabatic torsional dynamics at the conical intersection (J.P. Shaffer, M. Schmitt, T. Schultz, M.Z. Zgierski, I-C. Chen, M. Olivucci, A. Stolow, unpublished manuscript)—an inertial effect—and/or to a very subtle re-ordering of the conical intersections upon methylation (M. Olivucci, private communication)—an electronic effect. We speculated that this methyl group effect on C=C conical intersections seen in the α,β -enones is of a more general paradigm. If so, it is worthy of further investigation as these simple substitutions could be used to provide an important new type of control over the electronic branching ratios.

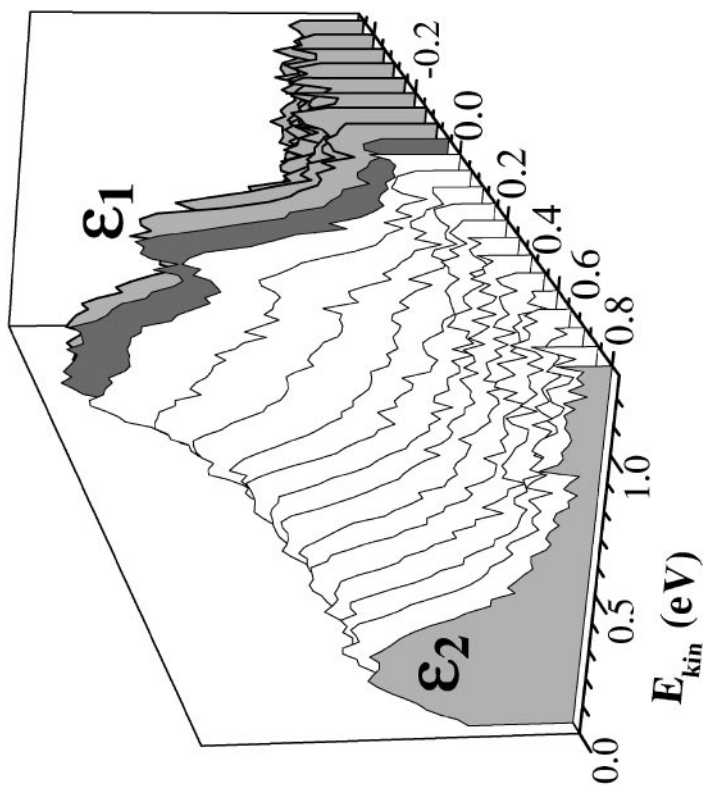
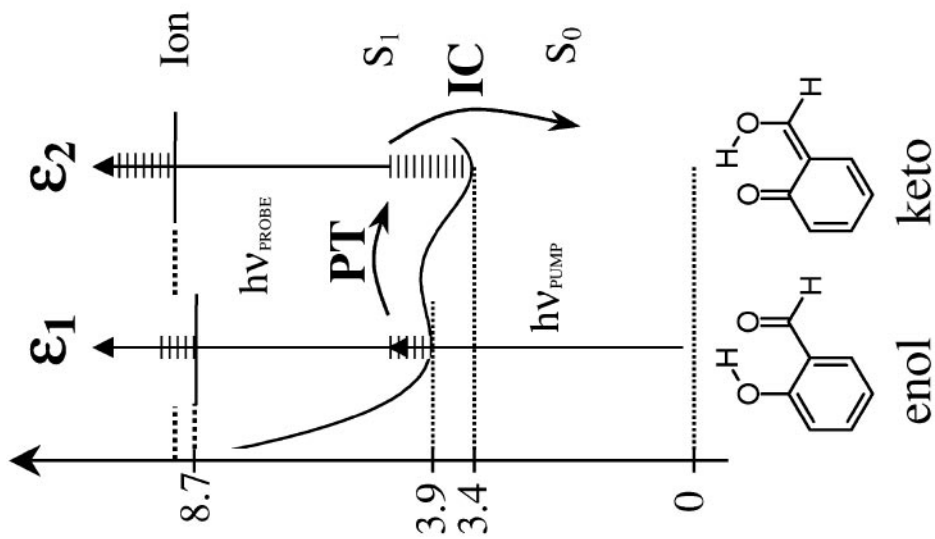
In the following sections, we give specific, more detailed examples of the application of TRPES to dynamical problems in proton transfer, photoisomerization, and photodissociation.

EXCITED STATE PROTON TRANSFER DYNAMICS

Proton transfer is one of the most important chemical processes (63). Excited state proton transfer in particular may play a role in protein binding, biomolecule fluorescence, and a range of applications including four-level lasers, photostabilizers, and data/energy storage (64). Excited state intramolecular proton transfer (ESIPT) processes are very important because they allow for a more detailed comparison of experiment with theory. Using a simple example, we discuss here the use of TRPES in elucidating both primary and secondary processes in ESIPT. *o*-Hydroxybenzaldehyde (OHBA) is the smallest aromatic molecule displaying ESIPT and was subject to numerous investigations in matrices (65) and in the liquid phase (66–68). Theoretical studies predicted a small (64) or nonexistent barrier (69, 70) for the proton transfer and suggested similar reaction dynamics for many ESIPT systems. We have used TRPES to study ESIPT in OHBA, the monodeuterated ODBA, and the analogous two-ring system hydroxyacetone naphthone (HAN) as a function of pump laser wavelength, tuning over the entire enol S_1 ($\pi\pi^*$) absorption band (71). The common timescale of ESIPT processes observed here and elsewhere (72) may indicate that the proton transfer “rate” is governed by the inertia of the involved ring modes and not by a transition rate over a barrier along the OH-coordinate.

The experimental scheme is depicted in Figure 8 (left), showing energetics for the case of OHBA. Excitation with a tunable pump laser $h\nu_{\text{pump}}$ forms the enol tautomer in the S_1 ($\pi\pi^*$) state. ESIPT leads to ultrafast population transfer from the S_1 enol to the S_1 keto tautomer. On a longer timescale, the S_1 keto population decays via internal conversion to the ground state (71). Both the enol and keto excited state populations are probed by ionization with a probe laser $h\nu_{\text{probe}}$, producing the two photoelectron bands ε_1 and ε_2 . The intensities of these two bands depended on both the pump-probe time delay and the pump laser wavelength. In Figure 8

Figure 8 (Left) Energetics for excited state proton transfer in OHBA, showing the enol and keto forms. Excitation with a pump laser $h\nu_{\text{pump}}$ forms the enol tautomer in the S_1 ($\pi\pi^*$) state. ESIPT leads to ultrafast population transfer from the S_1 enol to the S_1 keto tautomer. On a longer timescale, the keto S_1 population decays via internal conversion to the keto ground state. Both the enol and keto excited state populations are probed via ionization with a probe laser $h\nu_{\text{probe}}$, producing the two photoelectron bands ε_1 and ε_2 . (Right) TRPES spectra of OHBA at an excitation wavelength of 326 nm and a probe laser wavelength of 207 nm. Two photoelectron bands were observed: ε_1 due to ionization of the S_1 enol; ε_2 due to ionization of the S_1 keto. Band ε_1 was observed only when the pump and probe laser beams overlapped in time, indicating a sub-50 fs timescale for the proton transfer. Band ε_2 displayed a wavelength-dependent lifetime in the picosecond range corresponding to the energy dependent internal conversion rate of the dark S_1 keto state formed by the proton transfer. For a discussion, see the text.



(right), we present TRPES spectra of OHBA at an excitation wavelength of 326 nm. Two photoelectron bands ε_1 and ε_2 with distinct dynamics were observed. Band ε_1 is due to photoionization of the initially populated S_1 enol tautomer, band ε_2 to the photoionization of the S_1 keto tautomer. Both bands were observed across the whole absorption range (286–346 nm) of the S_1 state (71).

The decay of band ε_1 corresponds to the decay of the S_1 enol population and contains information about the proton transfer dynamics. We estimated an upper limit of 50 fs for the lifetime of the S_1 enol tautomer. Proton transfer reactions often proceed via tunnelling of the proton through a barrier, and deuteration of the transferred proton should then significantly prolong the lifetime of the S_1 enol tautomer. In experiments with ODBA, we did not observe an isotope effect—i.e., the ES IPT reaction was again complete within 50 fs. We concluded that the barrier in the OH stretch coordinate must be very small or nonexistent (71). This interpretation is supported by TDDFT ab initio calculations that predict no barrier for the proton transfer (69, 70). As is common in TRPES, these spectra also give insights into the dynamics on the dark state, in this case the S_1 keto state. The picosecond decay of band ε_2 corresponds to the loss of the S_1 keto population due to internal conversion to the ground state. The wavelength-dependent S_1 keto internal conversion rates in OHBA and ODBA likewise revealed no significant isotope effect (71). The measured internal conversion rates are very fast (1.6–6 ps over the range 286–346 nm) considering the large energy gap of 3.2 eV between the ground and excited state. It has been suggested that this is caused by the existence of a rate-determining barrier followed by an efficient conical intersection involving an OH bending mode (69, 70). The observed absence of an isotope effect on S_1 keto internal conversion in ODBA does not support this mechanism, but a conical intersection might be present along other modes, which do not involve vibrational motion of the active hydrogen atom. As discussed elsewhere, our results suggest that interactions with a nearby $n\pi^*$ state may play an important role in the keto internal conversion (62). This example serves to illustrate how TRPES can be used to study the dynamics of biologically relevant processes such as proton transfer and that it reveals details of both the proton transfer step and the subsequent dynamics in the dark state formed after the proton transfer.

PHOTOPHYSICS OF A PROTOTYPE MOLECULAR SWITCH

Active molecular scale electronics (3) involves the use of molecules as transistors, switches, modulators, etc. and requires a dynamical process that couples changes in optical or electrical properties to molecular rearrangements such as isomerization. As optical or electrical properties are governed by the electronic wavefunction, the underlying physical process is the nonadiabatic coupling of electronic with vibrational motions (73). It is the competition between fast molecular electronic processes—some desired, some not—which will govern the efficiency and stability of active molecular scale electronic devices, and therefore, the rational design of such devices should include considerations of excited state nonadiabatic

processes. Azobenzene (AZ) is often considered as the prototypical fast molecular electronic switch and its photoisomerization (74) is the basis for numerous functional materials, with applications in photonics (75, 76) and data storage (77), as triggers for protein folding (78) or as probes of local environment (79). Despite this great interest in azobenzene, the basic photoisomerization mechanism still remains unsolved (80): In contrast to the expectations of Kasha's rule, the isomerization quantum yields decrease rather than increase with increasing photon energy. In Figure 9 (top) we illustrate the two possible isomerization channels,

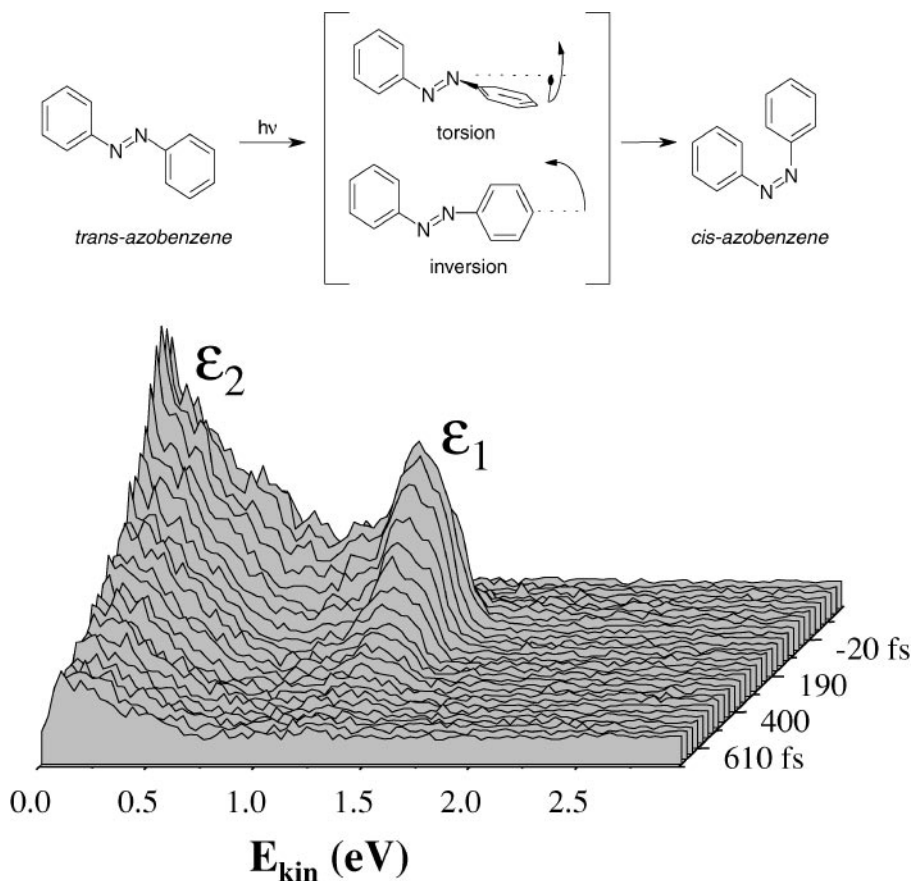


Figure 9 (Top) Photoisomerization dynamics of trans-azobenzene, indicating torsional and inversion pathways. (Bottom) TRPES spectra of trans-azobenzene excited at 330 nm and probed at 207 nm. Two photoelectron bands ϵ_1 and ϵ_2 were observed, having identical laser-limited risetimes but differing decay rates ($\tau_1 = 130$ fs, $\tau_2 = 410$ fs) and differing Koopmans' ionization correlations. These results indicate that there is a previously unrecognized $\pi\pi^*$ state, S_3 , involved in the dynamics, suggesting a new model of trans-azobenzene photoisomerization dynamics. For details see the text.

proceeding via either a planar pathway (“inversion”) or a nonplanar, twisted pathway (“torsion”). The investigation of quantum yields in several constrained azobenzenes determined that isomerization in the first excited state S_1 proceeds along the inversion coordinate (74). The second excited state S_2 is generally thought to be the N=N analogue of the C=C $\pi\pi^*$ -state in stilbene and that, somehow, motion along the torsional coordinate in S_2 is responsible for the observed reduction in isomerization yield. Recent time-resolved studies were interpreted within this model (81–88) and suggested that photoisomerization proceeds via the inversion coordinate in S_1 . The role of the torsional isomerization pathway remains controversial. Theoretical studies have supported both torsion and inversion pathways but disagreed on the states involved in the excited state relaxation (89, 90).

In Figure 9 (bottom) we show a time-resolved photoelectron spectrum for excitation of AZ to the origin of its S_2 state. Two photoelectron bands ε_1 and ε_2 with differing lifetimes and differing Koopmans’ correlations were observed (T. Schultz, M.Z. Zgierski, A. Stolow, et al., unpublished manuscript). Therefore, the ε_1 and ε_2 bands must be understood as arising from the ionization of two different electronic states. Furthermore, as both bands rise within the laser cross-correlation, they are caused by direct photoexcitation from S_0 and not to secondary processes. Therefore, in order to account for different lifetimes, different Koopmans’ correlations and simultaneous excitation from S_0 , we must invoke the existence of an additional state, S_3 , which overlaps spectroscopically with S_2 (T. Schultz, M.Z. Zgierski, A. Stolow, et al., unpublished manuscript). According to the Koopmans’ analysis (based upon assignment of the photoelectron bands) and to high level, large active space CASSCF calculations, this new state S_3 corresponds to $\pi\pi^*$ excitation of the phenyl rings (T. Schultz, M.Z. Zgierski, A. Stolow, et al., unpublished manuscript; T.J. Martinez, J. Quenneville, private communication). The π^* -excitation in the ring does not directly “break” the N=N bond and therefore might be expected to lead to reduced isomerization quantum yields. This mechanism differs greatly from that of all earlier models in that they always assumed that a single bright state, the S_2 (N=N $\pi\pi^*$) state, exists in this wavelength region (T. Schultz, M.Z. Zgierski, A. Stolow, et al., unpublished manuscript). This example shows how TRPES can be used to study competing electronic relaxation pathways in a model molecular switch and that it can reveal hidden yet highly important electronic states that can be hard to discern via conventional means.

NONADIABATIC PHOTODISSOCIATION DYNAMICS

The most interesting case for photochemistry is that of unbound excited states or excited states coupled to a dissociative continuum. The dissociative electronically excited states of polyatomic molecules can exhibit very complex dynamics, usually including nonadiabatic processes. These cases present a challenge to high-resolution spectroscopy as the spectra can often appear broad and

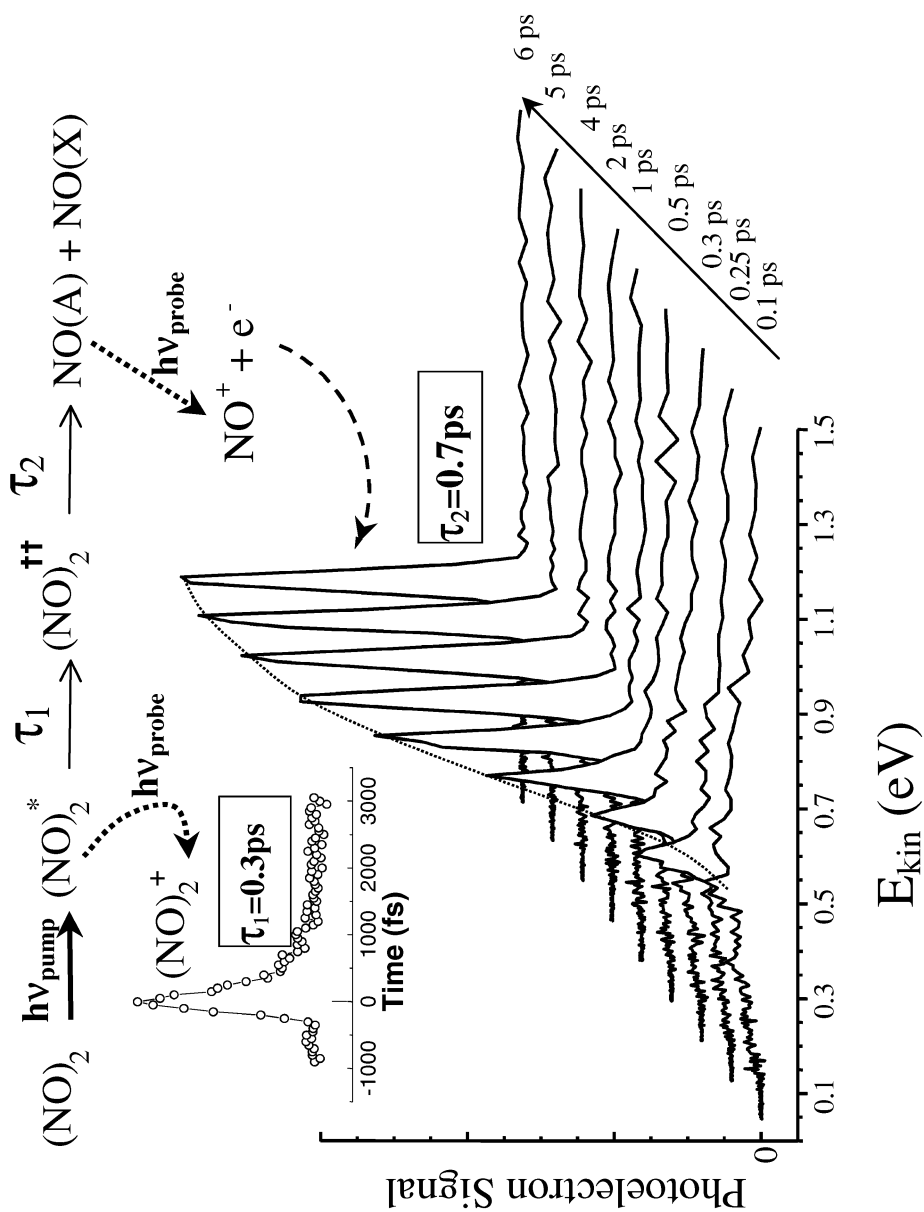
featureless. Measurements of product state distributions are likewise used to discern excited state dynamics. However, these may not be revealing of nonadiabatic couplings because they are sensitive to forces acting primarily in the product exit channel. We discuss here a TRPES study of the photodissociation dynamics of a polyatomic molecule, the *cis*-planar nitric oxide dimer, characterized by a diffuse absorption spectrum and a nearly statistical product state distribution, both of which conceal a more complex dynamics lying underneath (22). The UV absorption spectrum of (NO)₂ is broad and featureless, spanning the range 190–240 nm with a maximum at 205 nm, suggestive of a direct dissociation process. Broad, apparently featureless absorption spectra, however, can also arise from ultrafast nonadiabatic processes in the excited state whose timescale may be unrelated to the dissociation timescale. One can distinguish a direct from a step-wise nonadiabatic photodissociation process via a consideration of the effect of an evolving electronic symmetry on the photoionization dynamics using the TRPES method (22).

Studies of the (NO)₂ photodissociation dynamics at 193 nm revealed that two product channels are open (93):



At 193 nm, the energies available to channels (A) and (B) are 0.93 eV and 0.69 eV, respectively. The observed NO (A,B) product state distributions were quite broad. Subsequent studies on the alignment and vector correlations (94) of the excited state products showed only quite weak effects.

In Figure 10 (insert), we show a pump-probe measurement of the decaying (NO)₂⁺ parent ion signal as a function of time delay. The pump and probe wavelengths were 210 and 287 nm, respectively. A single exponential fit to the decay yields a time constant of 322 ± 12 fs. This might be interpreted (incorrectly) as the dissociation time of the excited state. In Figure 10, we also show femtosecond TRPES spectra for a series of time delays (22). The prominent feature is a sharp peak at 0.52 eV, which grows with time. This sharp peak is the well known Δ*v* = 0 NO(A²Σ⁺, *v*) → NO⁺(X¹Σ⁺, *v*) ionizing transition (95). Neither the ground state NO(X²Π) nor the excited state NO(B²Π) product are ionized at 287 nm: the former because of its high ionization potential, the latter because of its unfavorable electronic configuration for single photon, single active electron ionization. Interestingly, the appearance time of the NO(A) state product 0.52 eV peak is considerably slower (0.7 ps) than the disappearance time of the parent ion signal (0.3 ps). This surprising difference in timescales between excited parent signal disappearance and product signal appearance suggests a two-step nonadiabatic mechanism, rather than a direct mechanism as had been proposed. The nonadiabatic decay of the (NO)₂^{*} state on a timescale τ₁ ≈ 0.3 ps, is to another excited state, labelled (NO)₂^{††}, which has a relatively poor cross section for photoionization into the D₀ cation ground state, presumably due to an unfavorable electronic



configuration. This suggests why the parent ion signal decays in 0.3 ps even though the molecule has not yet dissociated. It is this second (dark) state that decays to the products on a longer timescale of $\tau_2 \approx 0.7$ ps. These results have recently been corroborated by detailed pump-probe 3D energy-angle resolved photoelectron-photoion coincidence-imaging studies of $(\text{NO})_2$ photodissociation dynamics (96; J.P. Shaffer, A. Stolow, C.C. Hayden, unpublished manuscript). It is important to note that these results show how the time-resolved integrated parent ion signal alone can be very misleading in polyatomic dissociation dynamics, because of changes in electronic symmetry during the dissociation.

CONCLUSIONS AND FUTURE DIRECTIONS

TRPES is emerging as a promising technique for the study of ultrafast excited state dynamics in polyatomic molecules. In this paper we have attempted to elucidate the important concepts in TRPES and to illustrate its applicability to different areas of nonadiabatic molecular dynamics. We have discussed general aspects of femtosecond pump-probe experiments from both the wavepacket and the frequency domain point of view. Experimentalists are, in principle, free to choose a final state through which to observe the wavepacket dynamics of interest. We have emphasized the critical role of the choice of final state in determining both the experimental technique (e.g., collection of photons or particles) and the information content of the experiment. Ideally, the final state should be sensitive to the complete excited-state dynamics (no dark states), and the observed signal can be dispersed (as in dispersed fluorescence or photoelectron spectroscopy) with respect to the set of final states within the laser bandwidth. We have argued (13) that photoelectron spectroscopy is well suited to the study of polyatomic dynamics because of its sensitivity to both electronic configurations and vibrational dynamics and the universal nature of photoionization as a probe. We considered the potential role of different electronic continua (i.e., ionization into different cation electronic states) in disentangling coupled electronic-vibration dynamics. We delineated two limiting cases for Koopmans'-type ionization correlations, giving an experimental

← **Figure 10** Nonadiabatic photodissociation dynamics of $(\text{NO})_2$ with a fs pump pulse at 207 nm and probe pulse at 287 nm. The dynamics were shown to be step-wise rather than direct, involving a dark configuration $(\text{NO})_2^{\ddagger\dagger}$ as the intermediate. (*Inset*) The $(\text{NO})_2^+$ parent ion signal as a function of time delay. A single exponential fit gives a time constant of $\tau_1 \sim 0.3$ ps. (*Main*) TRPES spectra with a prominent peak (0.52 eV) due to growth of the $\text{NO}(\text{A } ^2\Sigma^+, \nu)$ product with a $\tau_2 \sim 0.7$ ps time constant. The $\text{NO}(\text{A})$ appears more slowly than the disappearance of the excited parent molecule, indicating that the dissociation is nonadiabatic and occurs with at least two steps, as discussed in the text.

example of each type and discussed how they affected the information content of an experiment. We believe that TRPES will have applications in several areas of molecular reaction dynamics and attempted to illustrate this with three examples: excited state intramolecular proton transfer, photoisomerization dynamics, and nonadiabatic photodissociation dynamics. In each case, the TRPES method was able to shine new light on the problem, identifying the states and timescales involved and, particularly, giving a direct view of the dynamics on the dark states that may be difficult to obtain via other means.

Although we believe TRPES to be a powerful tool for the study of excited state nonadiabatic dynamics, as the dynamics becomes more complex and dissociative processes occur, it becomes a serious challenge to “follow” the dynamics from the initially prepared state all the way through to products. The only remaining possibility is to make multiply differential measurements of the product state attributes (e.g., energy and angular distributions and vector correlations based upon product angular momentum polarization) as a function of time and try to work backwards from the products toward the excited state dynamics. In collaboration with C.C. Hayden of Sandia National Labs who pioneered the method, we are measuring full 3D momentum recoil vectors of the ion and electron, recorded in coincidence using a pair of time and position sensitive MCP detectors and coincidence electronics (96; J.P. Shaffer, A. Stolow, C.C. Hayden, unpublished manuscript). These time-resolved correlation maps provide a novel way to follow chemical reaction dynamics from the initially excited state through to the final products, and they allow for unique time-resolved measurements of product state distributions and their various scalar and vector correlations.

ACKNOWLEDGMENTS

We thank our previous coworkers Prof. I. Fischer (Würzburg), Dr. M.J.J. Vrakking (Amsterdam), Dr. V. Blanchet (Toulouse), Dr. M. Lezius (Innsbruck), Dr. S. Lochbrunner (Munich), Dr. M. Schmitt (Würzburg), Prof. J.P. Shaffer (Oklahoma), Dr. J.J. Larsen (Aarhus), and Dr. D.M. Villeneuve (NRC) for their respective contributions. We thank our present coworkers Dr. T. Schultz (NRC), Dr. J.G. Underwood (NRC), Prof. T.J. Martinez (Illinois), Prof. I-C. Chen (Tsing-Hua) and Dr. S-H. Lee (Tsing-Hua), and Prof. M. Olivucci (Siena) for their important contributions to this work. We thank Prof. K. Müller-Dethlefs (York) for discussions on ZEKE spectroscopy and Prof. C.A. de Lange (Amsterdam) for discussions on magnetic bottle photoelectron spectroscopy. We thank Dr. C.C. Hayden (Sandia National Laboratories) for ongoing collaborations on 3D coincidence-imaging spectroscopy, Dr. T. Seideman (NRC) and Prof. K.L. Reid (Nottingham) for enlightening discussions and continuing collaborations on photoelectron angular distribution measurements, W. Domcke (Munich) for numerous helpful discussions, and Dr. M.Z. Zgierski (NRC) for ongoing collaborations on nonadiabatic dynamics in polyatomic molecules.

The Annual Review of Physical Chemistry is online at
<http://physchem.annualreviews.org>

LITERATURE CITED

1. Michl J, Bonacic-Koutecky V. 1990. *Electronic Aspects of Organic Photochemistry*. New York: Wiley
2. Schoenlein RW, Peteanu LA, Mathies RA, Shank CV. 1991. *Science* 254:412
3. Jortner J, Ratner MA. 1997. *Molecular Electronics*. Oxford, UK: IUPAC, Blackwell
4. Bixon M, Jortner J. 1968. *J. Phys. Chem.* 48:715
5. Jortner J, Rice SA, Hochstrasser RM. 1969. *Adv. Photochem.* 7:149
6. Henry BR, Siebrand W. 1973. Radiationless transitions. In *Organic Molecular Photophysics*, ed. JB Birks, 1:152. London: Wiley
7. Freed KF. 1976. Energy dependence of electronic relaxation processes in polyatomic molecules. In *Radiationless Processes in Molecules and Condensed Phases*, ed. FK Fong, p. 23. Berlin: Springer-Verlag
8. Stock G, Domcke W. 1997. *Adv. Chem. Phys.* 100:1
9. Kommandeur J, Majewski WA, Meerts WL, Pratt DW. 1987. *Annu. Rev. Phys. Chem.* 38:433
10. Schinke R. 1993. *Photodissociation Dynamics*. Cambridge, UK: Cambridge Univ. Press
11. Butler LJ. 1998. *Annu. Rev. Phys. Chem.* 49:125
12. Zewail AH. 2000. *J. Phys. Chem. A* 104:5660
13. Fischer I, Villeneuve DM, Vrakking MJJ, Stolow A. 1995. *J. Chem. Phys.* 102:5566
14. Fischer I, Vrakking MJJ, Villeneuve DM, Stolow A. 1996. *Chem. Phys.* 207:331
15. Seel M, Domcke W. 1991. *J. Chem. Phys.* 95:7806
- 16a. Engel V. 1991. *Chem. Phys. Lett.* 178:130
- 16b. Meier Ch, Engel V. 1993. *Chem. Phys. Lett.* 212:691
- 16c. Meier Ch, Engel V. 1994. *J. Chem. Phys.* 101:2673
- 16d. Meier Ch, Engel V. 1994. *Phys. Rev. Lett.* 73:3207
17. Kim B, Schick CP, Weber PM. 1995. *J. Chem. Phys.* 103:6903
18. Cyr DR, Hayden CC. 1996. *J. Chem. Phys.* 104:771
19. Assion A, Geisler M, Helbing J, Seyfried V, Baumert T. 1996. *Phys. Rev. A* 54:R4605-8
20. Greenblatt BJ, Zanni MT, Neumark DM. 1996. *Chem. Phys. Lett.* 258:523
21. Radloff W, Sert V, Freudenberg Th, Hertel IV, Jouvét C, et al. 1997. *Chem. Phys. Lett.* 281:20
22. Blanchet V, Stolow A. 1998. *J. Chem. Phys.* 108:4361
23. Blanchet V, Zgierski MZ, Seideman T, Stolow A. 1999. *Nature* 401:52
24. Reid KL. 1993. *Chem. Phys. Lett.* 215:25
25. Reid KL, Duxon SP, Towrie M. 1994. *Chem. Phys. Lett.* 228:351
26. Seideman T. 1997. *J. Chem. Phys.* 107:7859
27. Althorpe SC, Seideman T. 1999. *J. Chem. Phys.* 110:147
28. Reid KL, Field TA, Towrie M, Matousek P. 1999. *J. Chem. Phys.* 111:1438
29. Suzuki T, Wang L, Kohguchi H. 1999. *J. Chem. Phys.* 111:4859
30. Arasaki Y, Takatsuka K, Wang K, McKoy V. 1999. *Chem. Phys. Lett.* 302:363
31. Lee S-H, Tang K-C, Chen I-C, Schmitt M, Shaffer JP, et al. 2002. *J. Phys. Chem.* 106:89790
32. Müller-Dethlefs K, Schlag EW. 1991. *Annu. Rev. Phys. Chem.* 42:109
33. Zhang X, Smith JM, Knee JL. 1994. *J. Chem. Phys.* 100:2429

34. Lakshminarayan C, Knee JL. 1995. *J. Phys. Chem.* 99:1768
35. Baumert T, Thalweiser R, Gerber G. 1993. *Chem. Phys. Lett.* 209:29
36. Neumark DM. 2001. *Annu. Rev. Phys. Chem.* 52:255–78
37. Hayden CC, Stolow A. 2000. Nonadiabatic Dynamics studied by femtosecond time-resolved photoelectron spectroscopy. In *Advanced Physical Chemistry*, ed. C-Y Ng, 10:91–126. Singapore: World Sci.
38. Eland JHD. 1984. *Photoelectron Spectroscopy*. London: Butterworths
39. Seideman T. 2002. *Annu. Rev. Phys. Chem.* 53:41–65
40. Reid KL. 2003. *Annu. Rev. Phys. Chem.* 54:397–424
41. Suzuki T, Whitaker BJ. 2001. *Int. Rev. Phys. Chem.* 20:313
42. Deleted in proof
43. Stert V, Radloff W, Freudenberg Th, Noack F, Hertel IV, et al. 1997. *Europhys. Lett.* 40:515
44. Hanold KA, Garner MC, Continetti RE. 1996. *Phys. Rev. Lett.* 77:3335
45. Garner MC, Hanold KA, Sowa Resat MS, Continetti RE. 1997. *J. Phys. Chem. A* 101:6577
46. Davies JA, LeClaire JE, Continetti RE, Hayden CC. 1999. *J. Chem. Phys.* 111:1
47. Lochbrunner S, Larsen JJ, Shaffer JP, Schmitt M, Schultz T, et al. 2000. *J. Electron. Spectrosc. Relat. Phenom.* 112:183
48. Bernard JE, Alcock AJ. 1994. *Opt. Lett.* 19:1861
49. de Lange CA. 1995. Rotationally resolved resonance-enhanced multiphoton ionization photoelectron spectroscopy of diatomic hydrides. In *High Resolution Laser Photoionization & Photoelectron Studies*, ed. I Powis, T Baer, CY Ng, p. 195. New York: Wiley
50. Bandrauk AD, ed. 1994. *Molecules in Laser Fields*. New York: Dekker
51. Gavrilá M, ed. 1992. *Atoms in Intense Laser Fields*. San Diego: Academic
52. Zavriyev A, Fischer I, Villeneuve DM, Stolow A. 1995. *Chem. Phys. Lett.* 234:281
53. Stolow A. 1998. *Philos. Trans. R. Soc. London Ser. A* 356:345
54. Vrakking MJJ, Villeneuve DM, Stolow A. 1996. *Phys. Rev A* 54:R37
55. Blanchet V, Zgierski MZ, Stolow A. 2001. *J. Chem. Phys.* 114:1194
56. Schmitt M, Lochbrunner S, Shaffer JP, Larsen JJ, Zgierski MZ, Stolow A. 2001. *J. Chem. Phys.* 114:1206
57. Orlandi G, Zerbetto F, Zgierski MZ. 1991. *Chem. Rev.* 91:867–91
58. Petek H, Bell AJ, Yoshihara K, Christensen RL. 1991. *J. Chem. Phys.* 95:4739–49
59. Amirav A, Sonnenschein M, Jortner J. 1984. *J. Phys. Chem.* 88:5593
60. Shaffer JP, Schultz T, Schmitt M, Underwood JG, Stolow A. 2000. Untangling $\pi - \pi^*/n - \pi^*$ orbital interactions via time-resolved photoelectron spectroscopy. In *Springer Series in Chemical Physics, Ultrafast Phenomena XII*, ed. T Elsaesser, S Mukamel, M Murnane, N Scherer, 64:338–40. Berlin: Springer-Verlag
61. Deleted in proof
62. Deleted in proof
63. Douhal A, Lahmani F, Zewail AH. 1996. *Chem. Phys.* 207:477–97
64. Scheiner S. 2000. *J. Phys. Chem.* 104:5898–909
65. Morgan MA, Orton E, Pimentel GC. 1994. *J. Phys. Chem.* 94:7927
66. Nagaoka S, Hirota N, Sumitani M, Yoshihara K. 1983. *J. Am. Chem. Soc.* 105:4220
67. Nagaoka S, Nagashima U. 1989. *Chem. Phys.* 136:153
68. Catalán J, Toribio F, Acuña AU. 1982. *J. Phys. Chem.* 86:303
69. Sobolewski AL, Domcke W. 1994. *Chem. Phys.* 184:115
70. Sobolewski AL, Domcke W. 1999. *Phys. Chem. Chem. Phys.* 1:3065
71. Lochbrunner S, Schultz T, Schmitt M, Shaffer JP, Zgierski MZ, Stolow A. 2001. *J. Chem. Phys.* 114:2519

72. Lochbrunner S, Wurzer AJ, Riedle E. 2000. *J. Chem. Phys.* 112:10699
73. Brooks M, Brousseau R, Luong J, Charbonneau S, et al. 1999. *Phys. Can.* 55: 285
74. Rau H. 1990. Azo compounds. In *Photochromism: Molecules and Systems*, ed. HDürr, H Buas-Laurent, pp. 165–92. Amsterdam: Elsevier
75. Ikeda T, Sasaki T, Ichimura K. 1993. *Nature* 361:428
76. Cheben P, del Monte F, Worsfold DJ, Carlsson DJ, Grover CP, Mackenzie JD. 2000. *Nature* 408:64
77. Astrand P-O, Ramanujam PS, Hvilsted S, Bak KL, Sauer SPA. 2000. *J. Am. Chem. Soc.* 122:3482
78. Spörlein S, Carstens H, Renner C, Behrendt R, et al. 2002. *Proc. Natl. Acad. Sci. USA* 99:7998–8002
79. Kondo T, Yoshii K, Horie K, Itoh M. 2000. *Macromolecules* 33:3650
80. Tamai N, Miyasaka H. 2000. *Chem. Rev.* 100:1875
81. Nägele T, Hoche R, Zinth W, Wachtveitl J. 1997. *Chem. Phys. Lett.* 272:489
82. Lednev IK, Ye TQ, Hester RE, Moore JN. 1996. *J. Phys. Chem.* 100:13338
83. Lednev IK, Ye TQ, Matousek P, Towrie M, Foggi P, et al. 1998. *Chem. Phys. Lett.* 290:68
84. Lednev IK, Ye TQ, Abbott LC, Hester RE, Moore JN. 1998. *J. Phys. Chem.* 102: 9161
85. Biancalana A, Campani E, Di Donenico G, Gorini G, Iacoponi A, Masetti G. 1999. *Spectrochim. Acta* 55:2883
86. Biancalana A, Campani E, Di Donenico G, Gorini G, Masetti G. 1993. *J. Raman Spectrosc.* 24:43
87. Fujino T, Tahara T. 2000. *J. Phys. Chem. A* 104:4203
88. Fujino T, Arzhantsev SY, Tahara T. 2001. *J. Phys. Chem. A* 105:8123
89. Cattaneo P, Persico M. 1999. *Phys. Chem. Chem. Phys.* 1:4739
90. Ishikawa T, Noro T. 2001. *J. Chem. Phys.* 115:7503
91. Deleted in proof
92. Deleted in proof
93. Kajimoto O, Honma K, Kobayashi T. 1985. *J. Phys. Chem.* 89:2725
94. Naitoh Y, Fujimura Y, Honma K, Kajimoto O. 1995. *J. Phys. Chem.* 99:13652
95. Miller JC, Compton RN. 1981. *J. Chem. Phys.* 75:22
96. Shaffer JP, Schultz T, Underwood JG, Hayden CC, Stolow A. 2003. Time-resolved photoelectron spectroscopy: charge & energy flow in molecules. In *Springer Series in Chemical Physics, Ultrafast Phenomena XIII*. Vol. 71. Berlin: Springer Verlag. In press
97. Deleted in proof